Polymer Chemistry

ROYAL SOCIETY OF CHEMISTRY

PAPER

View Article Online
View Journal | View Issue

Cite this: *Polym. Chem.*, 2025, **16**, 3875

A multifaceted poly(ionic liquid)-based superabsorbent hydrogel for simultaneous removal of heavy metals and synthetic dyes

Patra Haripriya and Kari Vijayakrishna *

Water pollution remains a critical global concern, significantly intensified by rapid industrial development, agricultural runoff, and untreated urban discharges. In response to this environmental challenge, we have developed a poly(ionic liquid)-based hydrogel as a multifunctional and sustainable platform for simultaneous removal of heavy metals and organic dyes (both cationic and anionic) from wastewater. The hydrogels are synthesized *via* a one-pot polymerization–gelation process employing 2-acrylamido-2-methyl-1-propanesulfonic acid and vinyl imidazole as monomers. Quaternization of the imidazole moiety with 1,10-dibromodecane facilitated both crosslinking and ionic network formation. The resulting hydrogel, with 10% crosslinking density, demonstrated remarkable swelling capacity (2570%), indicating its superabsorbent nature. In rheological analysis, a dominant elastic behaviour with a coherent solid nature was observed for all the hydrogels. The FE-SEM study revealed a layered, interconnected structure with porosity in the interconnected region, signifying promising absorption potential. The hydrogels are explored towards the removal of carcinogenic heavy metals (Pb, Hg, Cd, Cr), and organic dyes. Due to the presence of both cationic and anionic polymer chains, these PIL-based hydrogels are found to be very effective in the removal of both cationic and anionic dyes from water medium. The hydrogel showed an absorption capacity of 250 mg g^{-1} and 490 mg g^{-1} of heavy metals and dyes, respectively. The recyclability and reusability make these hydrogels a sustainable material for removing carcinogenic materials from water bodies.

Received 10th June 2025,
Accepted 28th July 2025

DOI: 10.1039/d5py00584a

rsc.li/polymers

1. Introduction

Water is an essential resource for all life forms, yet water pollution has emerged as one of the most persistent environmental challenges of the modern era. Industrial effluents, untreated sewage, and discharges from pharmaceutical, textile, leather, polymer, and metallurgical industries introduce substantial quantities of toxic small molecules, synthetic dyes, and heavy metals (Pb, Hg, Cd, As) into aquatic ecosystems, causing severe ecological damage and posing significant health risks to humans, animals, and plants.[1–5] These pollutants are characterized by their high toxicity, non-biodegradability, and tendency for bioaccumulation, leading to critical health complications such as anemia, gastrointestinal issues, hypoglycemia, and, in extreme cases, mortality.[6–8] Traditional wastewater treatment techniques, including precipitation, coagulation and flocculation, adsorption, ion exchange, membrane filtration, and catalytic degradation, have been employed to mitigate this pollution; however, they often face inherent limitations in terms of long-term sustainability and effectiveness.[9–12] In this context, hydrogels have garnered increasing attention as versatile and promising materials to address the persistent shortcomings of conventional wastewater treatment methods.

Hydrogels are crosslinked hydrophilic polymer networks that absorb and retain significant amounts of water without dissolving.[13] The hydrophilic functional groups help in the absorption of water, and the crosslinking provides mechanical strength to keep the hydrogel structure intact.[14] In recent years, hydrogels have attracted huge research interest due to their simple method of preparation, tunable properties, and functionality. Hydrogels have a wide range of applications, including biomedical applications, tissue engineering, drug delivery, protein delivery, sensors, and soft contact lenses, as well as agriculture and wastewater treatment.[15–20] Hydrogels in their swollen state open up the free space between the network, allowing diffusion of any species with water. By incorporating specific functional groups in the polymer backbone, hydrogels can efficiently bind to heavy metal ions through chelation, ion exchange, or electrostatic interactions.[21,22] Similarly, their ability to entrap and encapsulate organic dyes through hydrogen bonding, hydrophobic interactions, and π–π

Department of Chemistry, Indian Institute of Technology Bhubaneswar-752050, Odisha, India. E-mail: kvijayakrishna@iitbbs.ac.in, vijayakrishnakari@gmail.com

stacking renders them highly effective in wastewater treatment applications.[23,24] Thus, the choice of monomer plays a crucial role in dictating the applicability of hydrogel.

Conventionally used monomers for hydrogel synthesis include acrylic acid, methacrylic acid, hydroxyethyl methacrylic acid, acrylate, acrylamide, *N*-isopropylacrylamide, ethylene glycol, ethylene glycol diacrylates, vinyl alcohol, styrene sulfonic acid and 2-acrylamido-2-methylpropane sulfonic acid.[25–27] These monomers have functional groups such as carboxyl, amide, sulfonic acid, and hydroxy groups, which boost the adsorption capacity of hydrogels through electrostatic interactions, hydrogen bonding, and chelation. Natural polymers such as alginate, chitosan, and cellulose derivatives have also gained attention due to their biodegradability and inherent metal-binding properties.[28,29] However, there are few reports on ionic liquids or poly(ionic liquid) (PIL) based hydrogels.[30]

Poly(ionic liquid) are a class of polyelectrolytes that combine the structural characteristics of conventional polymers with the distinctive properties of ionic liquids.[31,32] The versatility of PILs arises from their highly tunable molecular architecture, allowing for precise structural modifications to meet specific requirements. The ability to tailor functional groups and counter-ions within the polymeric framework enables the introduction of targeted physicochemical properties, making PILs highly adaptable for various advanced applications.[33–41] These uniqueness of PILs makes them choose as one of a suitable polymer system for hydrogels.

Conventional hydrogels have predominantly been investigated for single-application purposes. Our research interest lies in designing one-of-a-kind multifunctional hydrogel. Here, it is proposed to synthesize a poly(cationic-*co*-anionic) based hydrogel, in anticipation of their effectiveness towards the simultaneous removal of dyes (both cationic and anionic dyes) and heavy metals. To achieve our goal, we are strategically preparing a copolymer of vinyl imidazole and 2-acrylamido-2-methylpropane sulphonic acid, assuming the synthesized hydrogel system to show high swelling capacity and multiple applications. Here in this current report, the potential applications of synthesized hydrogels were explored towards the removal of carcinogenic substances like heavy metals and synthetic dyes from water.

2. Experimental section

2.1 Materials

1-Vinyl imidazole (≥99%), mercury(II) chloride ($HgCl_2$) (≥99%), lead(II) chloride ($PbCl_2$) (≥98%), cadmium(II) chloride ($CdCl_2$) (≥99.9%), chromium(III) chloride ($CrCl_3$) (≥99.9%), rhodamine B (≥95%), were procured from Sigma Aldrich and used as received. 1,10-Dibromodecane (≥97%), and rose bengal (≥98%) were purchased from Spectrochemical Pvt. Ltd and used as received. 2-Acrylamido-2-methyl-1-propanesulfonic acid (AMPS) was procured from TCI India. Congo red (≥98%) was purchased from Himedia and used as received. Methylene blue solution (aqueous) was purchased from Merck. 2,2-Azo bis(2-methyl propionamidine) dihydrochloride (>98%) (AAPH) was procured from SRL and used after recrystallizing it from methanol. Methanol and acetone were procured from Finar Ltd and used after distillation. All solutions were prepared using double-distilled water.

2.2 Synthesis of poly(ionic liquid) based hydrogel

1-Vinyl imidazole (1 g, 10.62 mmol), 2-acrylamido-2-methylpropane sulphonic acid (1 g, 5.31 mmol), and dibromodecane (0.32 g, 1.06 mmol) were dissolved in a minimum amount of water to prepare the monomer mixture. The monomer solution was sonicated for 15 minutes at room temperature to make it a clear solution and ensure uniform mixing. To the monomer mixture, AAPH (0.082 g, 0.32 mmol) initiator was added and stirred for 4 h at 65 °C to stimulate polymerization and gelation simultaneously. After the completion of reaction, the prepared hydrogel was first washed with methanol, followed by keeping it in distilled water for 24 h and replacing the water every 8 h. The cleaned hydrogel was dried under vacuum for 16 h at room temperature. A similar procedure was followed for the preparation of hydrogels by varying the amount of vinyl imidazole and crosslinker.

2.3 Characterization

The functional group identification for the hydrogels was determined by using FT-IR spectrometer (Bruker ALPHA-T, KBr pellet technique) in 4000–500 cm^{-1} wavenumber range with a 4 cm^{-1} resolution and 30 scans per measurement. The Shimadzu UV-1800 UV spectrophotometer operating within the wavelength range of 800–200 nm was used for UV studies. The surface morphology and elemental distribution analysis of the hydrogels were carried out using field emission scanning electron microscopy (FE-SEM, Zeiss Merlin, attached EDS Oxford X-Max Model: 51-XMX1004). For morphology analysis, samples are prepared using two methods. Initially, the sample was prepared by vacuum drying. To get a clearer idea about the morphology of the internal structure, the swelled hydrogel was submerged in liquid N_2 to crack open the layers. The cracked hydrogels were lyophilized, and the lyophilized hydrogel was mounted to carbon tape. Thermal analysis of the samples was carried out using a PerkinElmer STA 6000 instrument by taking 2–4 mg solid sample under nitrogen atmosphere with 10 °C min^{-1} temperature increment. The concentration of metal ions was determined using an Agilent ICP-OES-5100 instrument by taking 5 mL of liquid sample. Rheological analysis of the hydrogels was conducted in the swollen state at room temperature using an Anton Paar MCR 301 rheometer equipped with a cone-plate geometry (25 mm diameter, 2° angle). Oscillatory strain sweep measurements were performed over a strain range of 0.01% to 100% at a fixed angular frequency of 10 rad s^{-1} to determine the linear viscoelastic region. Frequency sweep analyses were conducted within the range of 0.01 to 100 rad s^{-1} at a constant strain of 0.5%. For all measurements, samples were prepared by dispersing 40 mg of dried powdered hydrogels in 3 mL of distilled water.

2.4 Swelling ratio

The swelling ratio of the hydrogels was determined by immersing the dry hydrogel in distilled water. The hydrogel was allowed to swell and achieve equilibrium swelling weight. The swelled hydrogel was taken out after a fixed time interval. The surface of the hydrogel was wiped with a filter paper to remove extra water and weighed. The swelling ratio (SR) percentage was calculated using the following equation[42]

$$SR\% = \left[\frac{(W_s - W_d)}{W_d}\right] \times 100 \quad (1)$$

where the W_s stands for swelled weight of hydrogel and W_d stands for dry weight of hydrogel.

2.5 Heavy metal entrapment

The heavy metal absorption efficiency of PIL-hydrogel was investigated. For the heavy metal absorption study, 50 ppm 50 mL aqueous solutions of Pb^{2+}, Hg^{2+}, Cd^{2+}, and Cr^{3+} was prepared separately and 20 mg of dry PIL-hydrogel was submerged into the heavy metal stock solution and kept for shaking at room temperature for 12 h. The swelled PIL-hydrogel was removed from the stock solution, dried in high vacuum for 16 h and analyzed using FE-SEM. The absorption capacity of hydrogel in multi-metal system was also carried out by submerging the hydrogel in two different stock solutions containing all four (Pb^{2+}, Hg^{2+}, Cd^{2+}, and Cr^{3+}) metal ions (12.5 ppm each and 50 ppm each). The experiments were performed in triplicate, and the mean values were reported.

2.6 Dye entrapment and removal

The dye entrapment study was carried out with both cationic (rhodamine B and methylene blue) and anionic (congo red and rose bengal) dyes. The stock solutions of both dyes were prepared by dissolving commercially available dyes in distilled water. The dye absorption experiment was conducted by passing the stock solution through 100 mg of dried PIL-hydrogel. The UV-Vis spectra were recorded to investigate the absorption of dye. The absorption efficiency of hydrogel towards a multicomponent dye system was also investigated by taking both methylene blue and rose bengal dye in one stock solution. The experiments were performed in triplicate, and the mean values were reported.

3. Results and discussion

3.1 Synthesis and characterization of poly(ionic liquid) based hydrogel

The intended hydrogels are copolymers of vinyl imidazole and 2-acrylamido-2-methylpropane sulfonic acid (AMPS), crosslinked using 1,10-dibromodecane (Scheme 1). Quaternization of the vinyl imidazole moieties was performed using 1,10-dibromodecane, which acted both as a cross-linking agent and as a source of the IL functionality, hence facilitating hydrogel formation. This approach of simultaneous polymerization and ionic liquid unit generation was followed from our previous report, where 1,10-dibromodecane crosslinked hydrogels showed excellent swelling.[43] 2-Acrylamido-2-methylpropane sulfonic acid was selected as a co-monomer due to its strong anionic sulfonic acid groups, which enhance the hydrogel's hydrophilicity and swelling capacity.[44] The sulfonic acid group is chemical resistant and can form strong hydrogen bonds, improving hydrogel's mechanical strength. The AMPS monomer is also biodegradable and biocompatible, which makes the hydrogel environmentally sustainable.[45,46] Polymerization of vinyl imidazole and 2-acrylamido-2-methylpropane sulfonic acid with 90% conversion yields a copolymer having average molecular weight of 7.2 kDa. But this copolymer without cross linking did not showed any gelation. On introduction of 1% and 3% of dibromodecane crosslinker, a similar result was observed. However, gelation is observed when the crosslinker percentage increases to 5%. The monomers and crosslinker ratios were optimized to prepare a superabsorbent hydrogel (Table S1). Hydrogels poly[$AMPS_{0.9}$-*co*-$VIm_{0.05}$/$VImDBr_{0.05}$] (**PIL-HG-1**), poly[$AMPS_{0.77}$-*co*-$VIm_{0.18}$/$VImDBr_{0.05}$] (**PIL-HG-2**), poly[$AMPS_{0.67}$-*co*-$VIm_{0.28}$/$VImDBr_{0.05}$] (**PIL-HG-3**), poly[$AMPS_{0.59}$-*co*-$VIm_{0.36}$/$VImDBr_{0.05}$] (**PIL-HG-4**), poly[$AMPS_{0.53}$-*co*-$VIm_{0.42}$/$VImDBr_{0.05}$](**PIL-HG-5**), poly[$AMPS_{0.5}$-*co*-$VIm_{0.45}$/$VImDBr_{0.05}$] (**PIL-HG-6**), and poly[$AMPS_{0.45}$-*co*-$VIm_{0.5}$/$VImDBr_{0.05}$] (**PIL-HG-7**) were prepared by varying the imidazole amount while keeping crosslinker percentage fixed (*i.e.*, 5%). Among all these hydrogels, **PIL-HG-4** exhibited good swelling in water. Thus, three hydrogels namely poly[$AMPS_{0.59}$-*co*-$VIm_{0.31}$/$VImDBr_{0.1}$] (**PIL-HG-8**), poly[$AMPS_{0.59}$-*co*-$VIm_{0.21}$/$VImDBr_{0.2}$] (**PIL-HG-9**), and poly[$AMPS_{0.59}$-*co*-$VIm_{0.21}$/$VImDBr_{0.3}$] (**PIL-HG-10**) were prepared by varying crosslinker density to 10%, 20%, and 30%, respectively (Table S1).

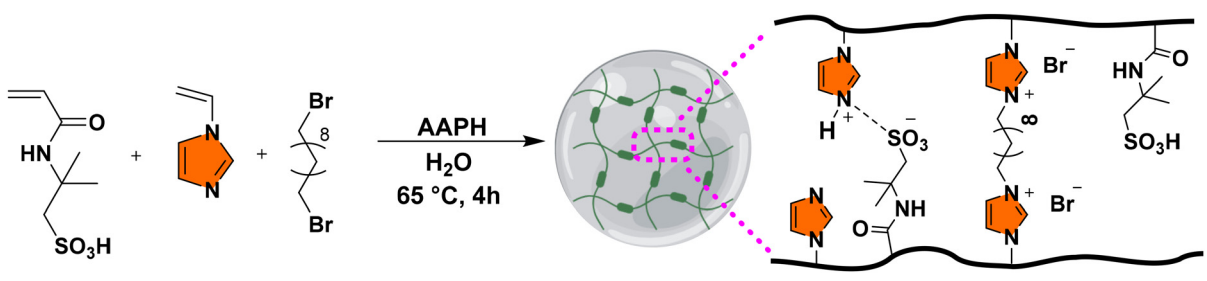

Scheme 1 Synthesis of PIL-based hydrogel.

The functional group identification for hydrogels (**PIL-HG-4**, **PIL-HG-8**, **PIL-HG-9**, and **PIL-HG-10**) was done using FT-IR (Fig. 1A). A broad peak centred at 3430 cm^{-1} is due to the O–H stretching of $–SO_3H$. The peaks at 2977 cm^{-1} and 2928 cm^{-1} are due to sp^{3-}C–H group and sp^{2-}C–H stretching, which appeared due to the long alkyl chain crosslinkers. The two broad peaks between 1647 cm^{-1} to 1554 cm^{-1} appeared due to amide-I peak (C═O stretching), merged with C═N stretching of imidazolium ring and amide-II peak (N–H bending). A mid-intense peak at 1465 cm^{-1} corresponds to C═C stretching frequency of aromatic carbon. The peak corresponds to symmetric bending of $–CH_2–$ merged with asymmetric stretching of S═O, appeared as an intense broad peak between 1305 cm^{-1} and 1200 cm^{-1}. Another low-intensity broad peak appeared at 1158 cm^{-1} and 628 cm^{-1} corresponds to the symmetric S═O stretching and S–O stretching, respectively.

The TGA thermograms of **PIL-HG-4**, **PIL-HG-8**, **PIL-HG-9**, and **PIL-HG-10** were shown in Fig. 1B. All the hydrogels followed three-step degradation patterns. The initial weight loss of 2–5% observed below 130 °C corresponds to the evaporation of physically absorbed water. The major degradation for **PIL-HG-4** was observed between 280–350 °C with maxima at 320 °C, corresponding to the decomposition of the polymeric backbone and crosslinked network. The second significant decomposition for hydrogel **PIL-HG-8**, **PIL-HG-9** and **PIL-10** was between 310–350 °C with a sudden weight loss of ≈60%. After 400 °C, all the hydrogels undergo steady weight loss, which involves decomposition of thermally stable residues like carbonaceous char. The DTA curve also showed the major degradation for **PIL-HG-4**, **PIL-HG-8**, **PIL-HG-9**, and **PIL-HG-10** was at 320 °C, 330 °C, 340 °C, and 345 °C respectively (Fig. S1). These results reveal that as the crosslinking density increases, the decomposition temperature slightly shifts to the higher side. This shows that the thermal stability of the hydrogels increases with an increase in crosslinking density.

The FE-SEM morphology reveals that the hydrogel surface has interconnected network structures, and the interconnection region has well-defined pores with variable shape and size (Fig. 1C). The surface appears relatively smooth, indicating uniform gelation. Whereas the interconnected porosity indicates successful phase separation during gelation. It plays a pivotal role in defining hydrogel's internal structure, enhancing its mechanical strength and swelling behaviour, thus making it suitable for absorption/desorption of drugs, metal ions, dyes, and small molecules.[47–49] When the hydrogel was cracked open using liquid N_2, a porous morphology was

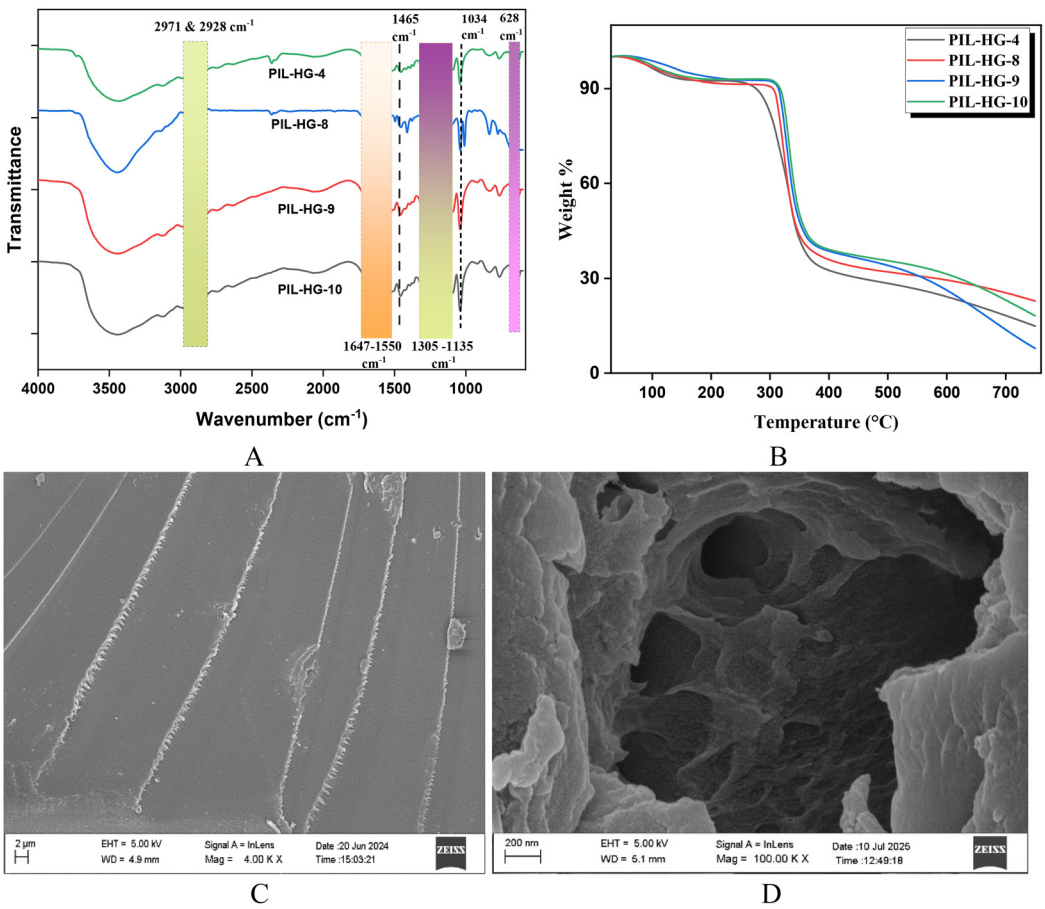

Fig. 1 (A) FT-IR overlay, (B) TGA curve overlay of poly(ionic liquid) based hydrogels with different crosslinker ratios, and (C) & (D) FE-SEM images of **PIL-HG-8**.

observed (Fig. 1D). This porous morphology with uniformity of the network and absence of significant agglomeration implies good structural integrity and efficient crosslinking in the hydrogel matrix.

The rheological behaviour of the hydrogels was analyzed in distilled water at room temperature. Oscillatory sweep and frequency sweep tests were conducted to evaluate the storage modulus (G') and loss modulus (G'') of **PIL-HG-4**, **PIL-HG-8**, **PIL-HG-9** and **PIL-HG-10**. Oscillatory sweep measurement shows that the storage modulus is higher than the loss modulus for all the hydrogels, indicating a predominant elastic behaviour and a well-developed three-dimensional polymeric network structure. The G' and G'' values increase as the percent crosslinking increases from 5% to 20%, indicating increased elastic properties with crosslinking. However, on further increase in crosslinking to 30%, the G' and G'' decreased due to over-crosslinking and network defects. The oscillatory sweep measurement also reveals that the linear viscoelastic region (LVR) for all the hydrogels is between 0.1 to 1% (Fig. 2A). The linear viscoelastic region is the range of applied stress within which the G' remains constant, indicating that the material's structure is not disrupted.[50] For all four hydrogels, a gradual decrease in the G' value is observed beyond the linear viscoelastic region (LVR), which is attributed to the disruption of polymer chain entanglements as shear stress increases.

The frequency sweep test was performed to evaluate the viscoelastic behaviour of hydrogels. The storage modulus (G') and loss modulus (G'') were measured across a frequency range (ω) from 0.1 rad s^{-1} to 100 rad s^{-1} with a constant shear stress of 0.5% for **PIL-HG-4**, **PIL-HG-8**, **PIL-HG-9** and **PIL-HG-10** (Fig. 2B). The frequency sweep shows that G' consistently surpasses G'' across the applied frequency range, indicating a coherent gel state. The frequency sweep model also shows that G'/G'' increases as the crosslinker amount increases to a specific concentration, and beyond that concentration again decreases. The absence of a crossover point between G' and G'' supports the hydrogel's solid-like nature. This concludes that all the hydrogels have a dominant elastic behaviour with a coherent solid-nature over a broad frequency (0.1 rad s^{-1} to 100 rad s^{-1}) and shear stress (0.01% to 100%) range. However, at higher strain, the hydrogel network is sensitive to deformation.

3.2 Swelling ratio and swelling kinetic study

A systematic swelling study was carried out for all the synthesized hydrogels. The equilibrium swelling ratio for all the hydrogels (**PIL-HG-1 to PIL-HG-10**) was presented in a table (Table S2). Fig. 3A shows the equilibrium swelling ratio for **PIL-HG-1**, **PIL-HG-2**, **PIL-HG-3**, **PIL-HG-4**, **PIL-HG-5**, **PIL-HG-6** and **PIL-HG-7**. The swelling ratio exhibits a non-linear trend, initially increasing with an increase in the concentration of imidazolium monomer, attaining a maximum, and again decreasing with a further increase in the concentration of imidazolium monomer. The increase in the swelling ratio from 940% (**PIL-HG-1**) to 1450% (**PIL-HG-4**) suggests that, on introduction of ionic character, the water intake ability of hydrogel increases due to osmotic pressure and electrostatic repulsion between the networks.[51–53] However, beyond a certain composition (*i.e.*, $AMPS_{0.59}$-$VIm_{0.36}$/$VImDBr_{0.05}$) the swelling ratio again decreases. This decrease in the swelling ratio may be attributed to excessive ionic crosslinking or a higher degree of chain entanglement, restricting network expansion, which reduces the water intake. Further, to understand the role of crosslinker, swelling ratio of **PIL-HG-8**, **PIL-HG-9** and **PIL-HG-10** were determined in distilled water (Fig. 3B). The hydrogel **PIL-HG-8** having 10% crosslinking, exhibits the highest swelling of 2570% classifying it as a superabsorbent hydrogel among all. In contrast, hydrogels with both lower and higher crosslinking percentages show a lower swelling ratio. The observed swelling ratio implies that PIL has a subtle influence, and the percentage of crosslinker has a drastic influence over the hydrogel swelling ability. Further, to understand the water intake mechanism, swelling kinetics of **PIL-HG-4**, **PIL-HG-8**, **PIL-HG-9**, and **PIL-HG-10** were carried out (Fig. S2A).

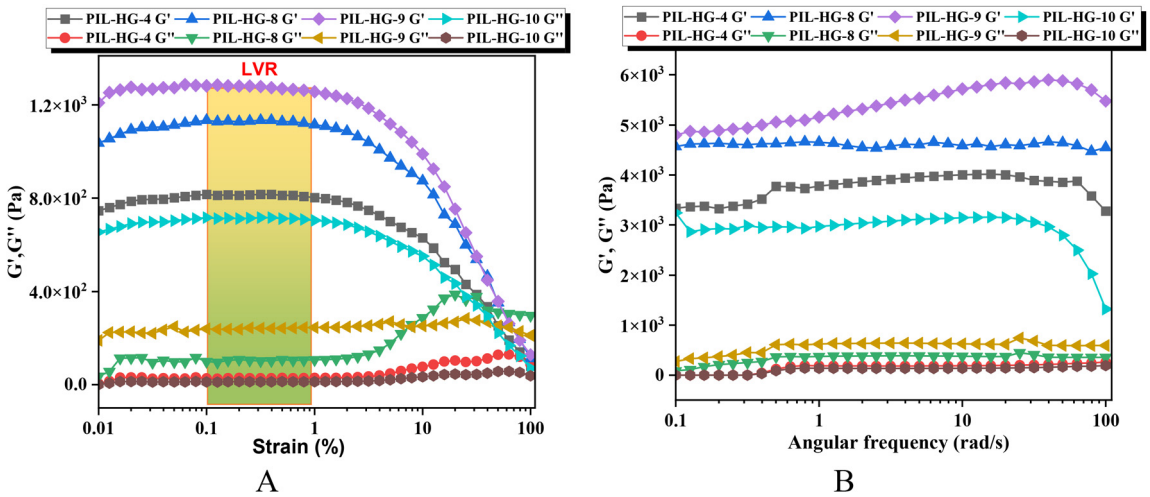

Fig. 2 Plot of (A) G', G'' *vs.* strain (B) G', G'' *vs.* angular frequency for **PIL-HG-8**.

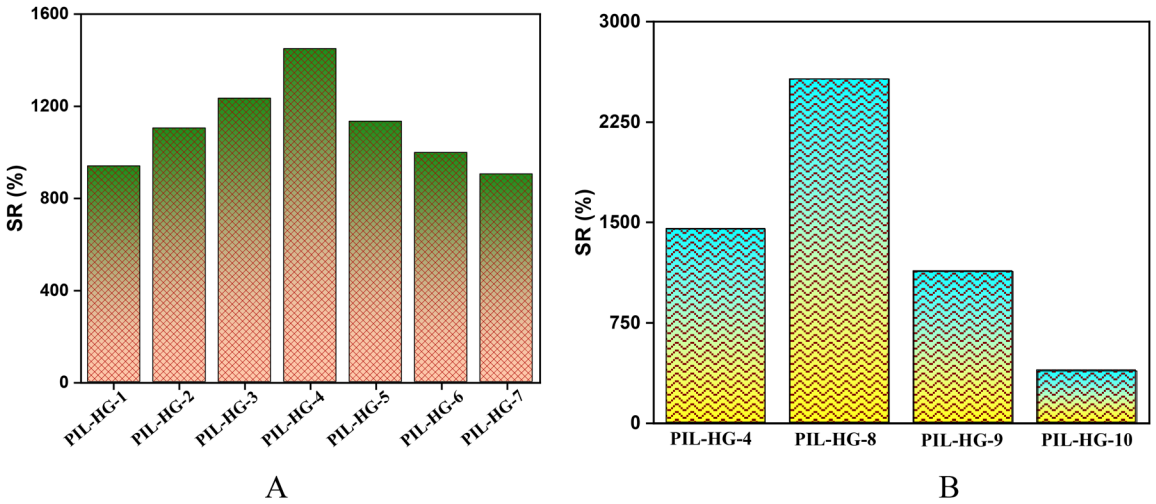

Fig. 3 (A) Equilibrium swelling ratio and (B) swelling kinetics of poly(ionic liquid) based hydrogels.

All the hydrogels initially show a rapid increase in swelling ratio, followed by a gradual approach towards equilibrium, indicating a diffusion control mechanism. The swelling ratio was calculated using another parameter R, which is expressed as following equation

$$R = \left(\frac{\omega_t}{\omega_0} - 1\right) \quad (2)$$

W_0 is the weight of dry hydrogel and W_t is the weight of hydrogel at time t.

The obtained data were fitted using Ritger-Peppas model using the following equation

$$R(t) = kt^n \quad (3)$$

Here, $R(t)$ represent swelling ratio at time t, k represents swelling rate constant or swelling rate front factor, t is time expressed in seconds and 'n' is diffusion exponent. The diffusion exponent (n) was calculated from the slope of the plot of $\log R$ *versus* $\log t$. An n value of 0.5 indicates Fickian diffusion, while values between 0.5 and 1.0 suggest a non-Fickian mechanism within the hydrogel matrix.[54,55] Fig. S2B represents the Ritger-Peppas model fit for hydrogels. The 'n' from Ritger-Peppas fitting for hydrogels **PIL-HG-4**, **PIL-HG-9**, and **PIL-HG-10** was found to be 0.178–0.176, which suggests a quasi-Fickian behaviour of hydrogels, where the diffusion process is dominant but has some contribution from relaxation (Table S3). However, the 'n' (0.096) value for **PIL-HG-8** suggests an intense diffusion-controlled swelling.

The swelling kinetics were further analysed using the following pseudo second-order kinetics model.

$$\frac{t}{q_t} = \frac{t}{q_e} + \frac{1}{k_2 {q_e}^2} \quad (4)$$

In this equation, q_t is swelling ratio at time t, q_e is equilibrium swelling ratio, t is time and k_2 is 2nd order rate constant. The plot between t/q_t *vs.* t shows a linear fit with all hydrogels (Fig. S2C). The rate constant and the equilibrium swelling ratio were calculated from the intercept and slope of the t/q_t *vs.* t plot (Table S4). **PIL-HG-8** shows an intermediate slope (3.848) and intercept (1.60), indicating rapid and high-capacity swelling. In contrast, the **PIL-HG-4** (6.384) and **PIL-HG-9** (8.153) showed higher slope, suggesting slower diffusion kinetics due to lower or higher crosslinking density.[56,57] Thus, **PIL-HG-8** with an optimum structural stability and highest swelling ratio, was used to check its applicability in absorption of heavy metals and synthetic dyes.

3.3 Heavy metal absorption

Heavy metal toxicity is an alarming environmental concern as it has serious health hazards for aquatic and terrestrial animals and plants due to its bioaccumulation and non-biodegradable nature. Metals such as lead, mercury, cadmium, chromium, *etc*. are carcinogenic and cause severe damage even in ppm levels. Because of the seriousness of heavy metal toxicity, the synthesized poly(ionic liquid) hydrogel was explored for heavy metal adsorption. **PIL-HG-8** was used for this study as it has the highest degree of swelling (*i.e.*, 2570%). The absorption capacity of the **PIL-HG-8** towards heavy metals was determined by taking Pb, Hg, Cd, and Cr salts in aqueous medium. The absorption efficiency of **PIL-HG-8** for individual metal ions, Pb^{2+}, Cd^{2+}, Cr^{3+}, and Hg^{2+} was found to be 249.21, 235.22, 246.20 and 246.96 mg g^{-1}, respectively (Fig. 4A). The result reveals that for individual mono-metallic systems, **PIL-HG-8** shows non-specific behaviour, which is beneficial for removing a broad range of metals. Most importantly, the **PIL-HG-8** shows a higher metal ion absorption for all four metal ions (Pb^{2+}, Cd^{2+}, Cr^{3+}, & Hg^{2+}) compared to the reported values for similar type of hydrogels (Table S5). The higher absorption capacity of **PIL-HG-8** was due to the presence of multi-metal-coordinating sites [SO_3H, SO_3^-, imidazole group, and poly(ionic liquid) moiety generated during quaternization of imidazole]. The smooth, uniform surface of **PIL-HG-8**

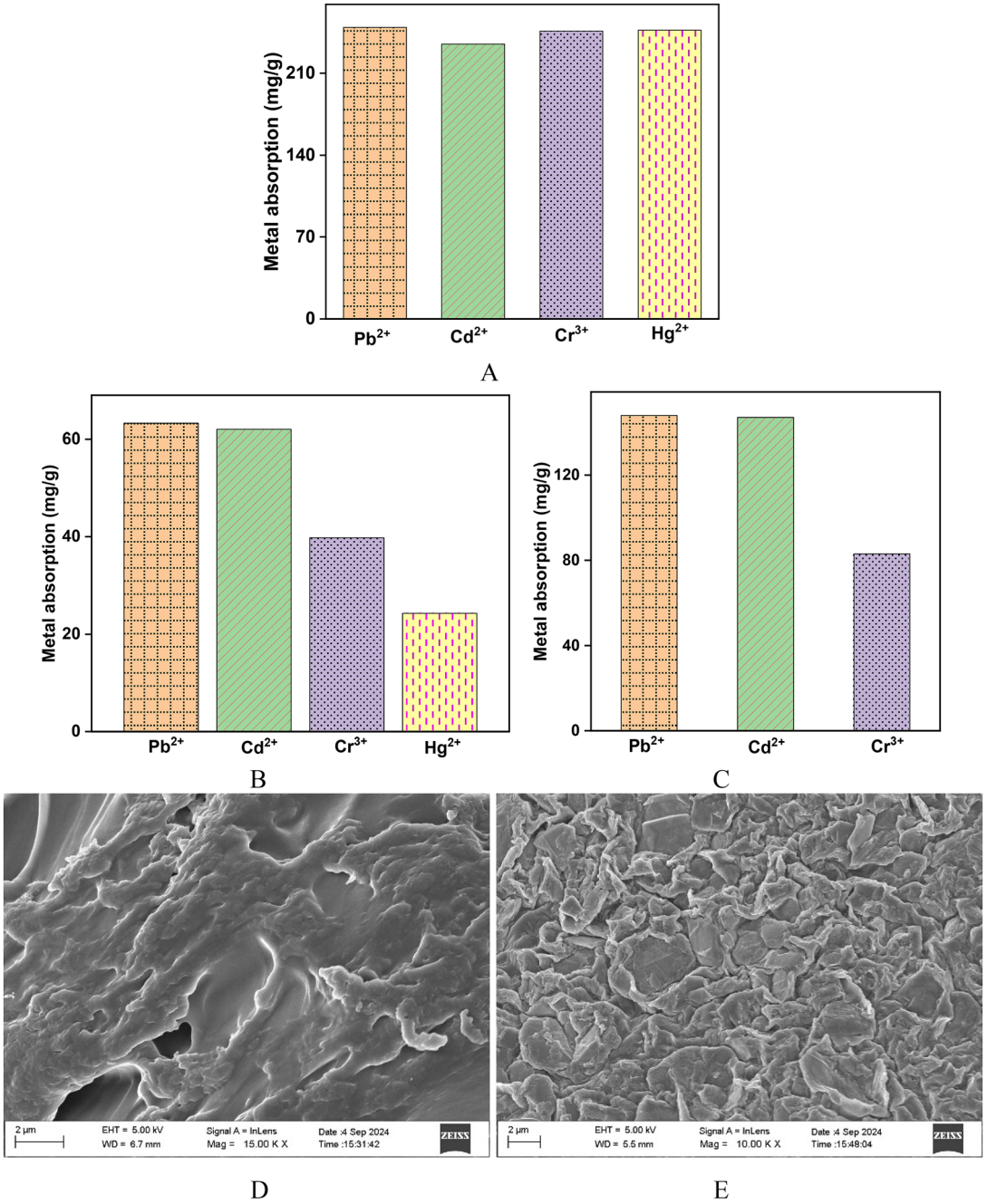

Fig. 4 Heavy metal absorption capacity of **PIL-HG-8** investigated in (A) mono-metallic system; multi-metallic system with (B) 12.5 ppm each metal, (C) 50 ppm each metal, and FE-SEM image of **PIL-HG-8** after absorption in solution containing (D) 12.5 ppm of each metal, (E) 50 ppm of each metal.

changes to irregular morphology, which results from the occupancy of metal ions in the hydrogel matrix. The elemental analysis also confirms the absorption of heavy metals (Fig. S3A–D).

To understand the absorption behaviour of **PIL-HG-8** in a multicomponent system, **PIL-HG-8** was submersed in a multicomponent system (**MCS-1**) having 12.5 ppm of each metal ion (Pb^{2+}, Cd^{2+}, Cr^{3+}, & Hg^{2+}) *i.e.*, resulting in an overall 50 ppm solution. The absorption capacity of **PIL-HG-8** for each metal ion was found to be 62.29, 62.00, 39.77, and 24.89 mg g^{-1} for Pb^{2+}, Cd^{2+}, Cr^{3+}, and Hg^{2+}, respectively (Fig. 4B). The surface morphology of the hydrogel also changed as the metal ions occupied the hydrogel network (Fig. 4D). The EDS analysis additionally confirms the adsorption of all four metal ions (Pb^{2+}, Cd^{2+}, Cr^{3+}, & Hg^{2+}) (Fig. S4A). To understand the competitive absorption of metal ions, the absorption capacity of the hydrogel **PIL-HG-8** was determined in another multicomponent system (**MCS-2**) containing all four metal ions [*i.e.*, Pb^{2+}, Cd^{2+}, Cr^{3+}, & Hg^{2+} (50 ppm each)]. The absorption capacity of

PIL-HG-8 for each metal in **MCS-2** was found to be 148.45, 147.18, and 83.33 mg g^{-1} for Pb^{2+}, Cd^{2+}, and Cr^{3+}, respectively (Fig. 4C). To our surprise, **PIL-HG-8** hydrogel did not absorb Hg^{2+} from the solution. The EDS analysis also confirms the absence of Hg^{2+} in the **PIL-HG-8** matrix (Fig. S4B). The surface morphology of the hydrogel after metal absorption has changed

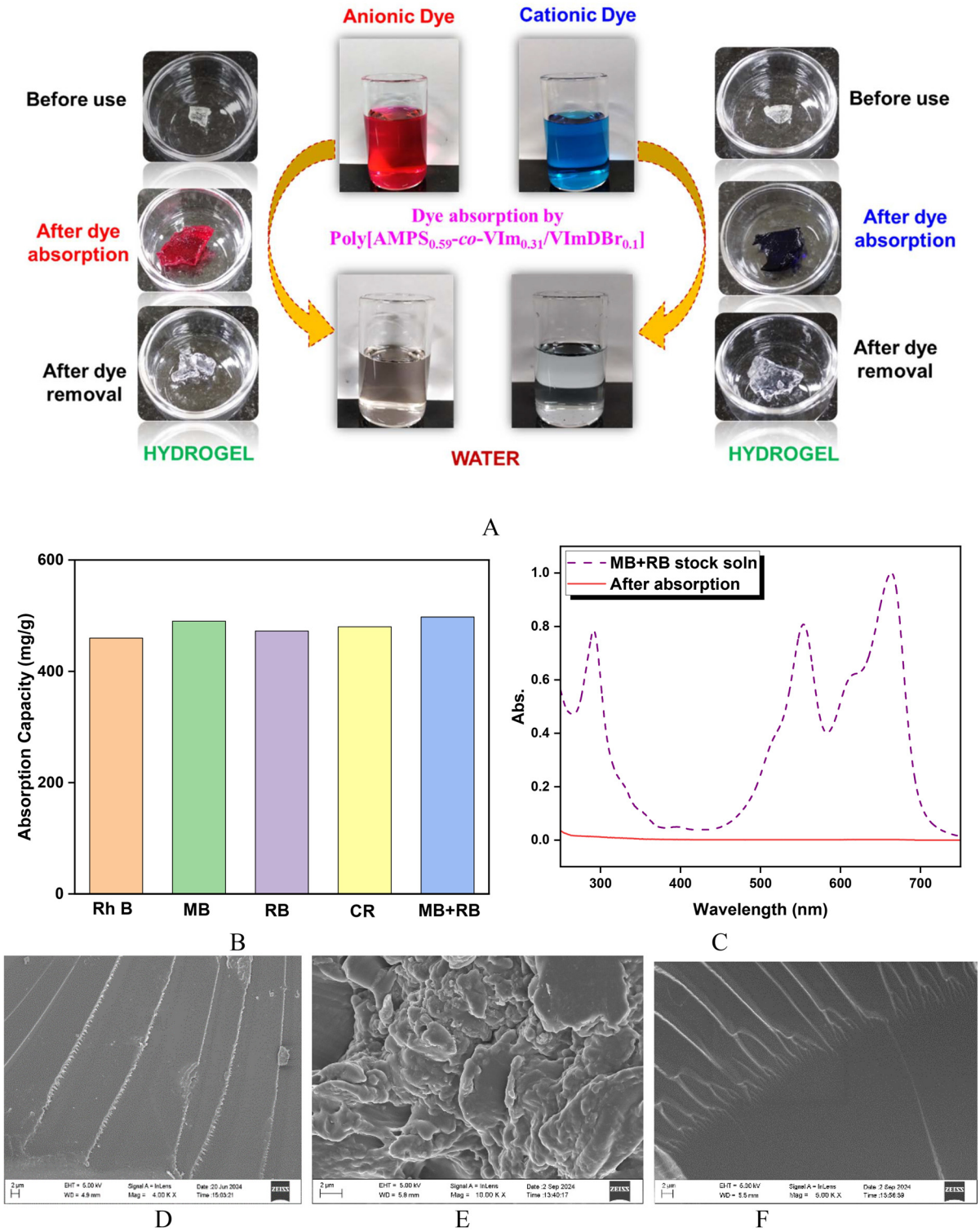

Fig. 5 (A) A digital image representation of both cationic and anionic dye absorption by **PIL-HG-8** (B) absorption capacity of **PIL-HG-8** for different dyes, (C) UV-Vis spectra of the combined absorption of MB and RB by **PIL-HG-8**, FE-SEM image of **PIL-HG-8** (D) before absorption, (E) after absorption, (F) after dye removal.

notably (Fig. 4E). The total absorption capacity of the **PIL-HG-8** from the **MCS-2** absorption was found to be 378.96 mg g^{-1} (the quantity of absorbed metals from the mixture of metal ions), which is much higher than the maximum absorption observed in a single metal ion system (Fig. 4A).

The single metal absorption by **PIL-HG-8** indicates the absorption capacity of metal ions follows the trend $Pb^{2+} \gtrsim Cr^{3+} \gtrsim Hg^{2+} > Cd^{2+}$. The absorption of multicomponent systems, where competition is expected, follows the order $Pb^{2+} \approx Cd^{2+} > Cr^{3+} > Hg^{2+}$. These results indicate that in multicomponent systems (**MCS-1** & **MCS-2**), the absorption affinity of **PIL-HG-8** is higher for Pb^{2+}, Cd^{2+}, and Cr^{3+}, with Hg^{2+} being least competitive among all. In **MCS-1**, where the concentration of metal ions was low (12.5 ppm each), due to the availability of absorption sites, all metal ions were absorbed. However, **MCS-2**, the absence of Hg^{2+} in the hydrogel matrix, may be due to the saturation of available metal ion binding sites in the hydrogel matrix. Furthermore, the elevated absorption levels of Pb^{2+} and Cd^{2+} observed in **MCS-1** and **MCS-2** indicate that these metal ions may possess competitive advantages in absorption behaviour compared to other metal ions.

3.4 Dye entrapment

Methylene blue (MB), Rhodamine B (Rh B), Congo red (CR) and rose Bengal (RB) are widely used in many industries. These dyes are carcinogenic, and dye-contaminated wastewater poses a significant environmental threat due to its toxic, persistent, and non-biodegradable nature. Due to the industrial importance and significant toxicity of synthetic dyes, the absorption capacity of poly(ionic liquid)-based hydrogels towards such dyes was investigated. Since the **PIL-HG-8** exhibited the highest swelling (*i.e.*, 2570) among all the hydrogels, it was used for dye absorption. The efficiency of **PIL-HG-8** was investigated towards both cationic (Rh B & MB) and anionic (CR & RB) dyes. The stock solutions of each dye were passed through **PIL-HG-8** individually, and the absorption was monitored by UV-Vis spectroscopy (Fig. S5A–D). The equilibrium absorption capacity of **PIL-HG-8** for Rh B, MB, RB and CR was found to be 460.50, 490.21, 472.8 and 480.20 mg g^{-1} respectively (Fig. 5B). **PIL-HG-8** is highly efficient for cationic and anionic dyes. A digital image representation of dye absorption of **PIL-HG-8** is presented in Fig. 5A.

To mimic the polluted water environment, both cationic (MB) and anionic (RB) dyes were combined and passed through the **PIL-HG-8**. The UV-Vis study reveals that the hydrogel shows high efficiency towards both the dyes (MB & RB) [Fig. 5C]. The equilibrium absorption capacity of **PIL-HG-8** in multicomponent system was found to be 497.50 mg g^{-1} (Fig. 5B). This observation may be attributed to the ionic moiety (SO_3H, SO_3^-, and quaternized imidazolium group) present in the hydrogel matrix, which has the potential to interact with both cationic and anionic dyes. Along with electrostatic interactions, other interactions like hydrogen bonding, hydrophobic interactions, and π–π interactions also facilitate the dye absorption capacity of **PIL-HG-8**. The surface morphology of **PIL-HG-8** before and after dye absorption was analyzed by FE-SEM. Before dye absorption, the morphology of the hydrogel is smooth and uniform (Fig. 5D). Upon absorption of dyes, the smooth and porous morphology is notably altered due to the occupancy of dyes (Fig. 5E). The surface morphology could be revert back after regenerating it by treatment with 5% HCl (Fig. 5F). The regenerated **PIL-HG-8** can be reused for 20 cycles without compromising its efficiency, making it a sustainable material for dye entrapment.

4. Conclusions

We have successfully synthesized the desired poly(ionic liquid) based hydrogel using vinyl imidazole and 2-acrylamido-2-methyl-1-propanesulfonic acid with a simple one-pot polymerization gelation technique. 1,10-Dibromodecane used to quaternize the imidazole group, which brings the poly(ionic liquid) nature, and the dodecyl chain provides the covalent crosslinking to the hydrogel matrix. Among all the synthesized hydrogels, **PIL-HG-8** becomes a superabsorbent hydrogel with the highest swelling ratio of 2570%. The hydrogel **PIL-HG-8** was employed for the removal of carcinogenic dyes, and heavy metals from contaminated water. **PIL-HG-8** displays a broad-spectrum absorption capacity of 249.21, 235.22, 246.20, and 240.96 mg g^{-1} for Pb^{2+}, Cd^{2+}, Cr^{3+}, and Hg^{2+}, respectively in a monometallic system. The non-specific broad absorption ability makes **PIL-HG-8** a green choice for removing toxic heavy metals (Pb^{2+}, Cd^{2+}, Cr^{3+}, and Hg^{2+}). **PIL-HG-8** shows a maximum absorption capacity of 378.96 mg g^{-1} (for a multicomponent system), which is a very high absorption among similar types of hydrogels. Along with heavy metals, **PIL-HG-8** is also active towards both cationic (methylene blue, and rhodamine B) and anionic (congo red, and rose bengal) dye absorption. In the single-component system equilibrium absorption capacity of **PIL-HG-8** was found to be 460.50, 490.21, 472.8 and 480.20 mg g^{-1} for Rh B, MB, RB and CR, respectively. In a multi-component of MB and RB, **PIL-HG-8** has a maximum absorption capacity of 497.5 mg g^{-1}. The dye-absorbed **PIL-HG-8** was easily regenerated by washing it with 5% HCl and reused up to 20 cycles without losing its efficiency. The hydrogel, **PIL-HG-8**, represents a unique, one-of-a-kind multifunctional material that provides a sustainable and environmentally friendly solution for clean water by removing heavy metals and synthetic dyes, aligning with the United Nations' Sustainable Development Goal 6.

Author contributions

Kari Vijayakrishna: conceptualization, supervision, resources, writing – reviewing and editing. Patra Haripriya: investigation, methodology, original draft preparation.

Conflicts of interest

Authors do not have any conflicts of interest.

Data availability

The data supporting this article provided in the SI.

Supplementary information containing compounds characterization and their swelling kinetics is available. See DOI: https://doi.org/10.1039/d5py00584a

Acknowledgements

Kari thanks DST-SERB, India (Project NO: CRG/2020/003754) for the financial support. Authors also thank IIT Bhubaneswar for the infrastructure and research facility. HP thanks IIT Bhubaneswar for fellowship.

References

1 F. M. M. Tchieno and I. K. Tonle, *Rev. Anal. Chem.*, 2018, **37**, 1–26.
2 M. H. A. Hussain and G. S. P. Soylu, *ACS Omega*, 2025, **10**, 9962–9975.
3 J. Si, S. Zhang, X. Liu and K. Fang, *Langmuir*, 2022, **38**, 6004–6012.
4 J. M. Millican and S. Agarwal, *Macromolecules*, 2021, **54**, 4455–4469.
5 R. Fried, I. Oprea, K. Fleck and F. Rudroff, *Green Chem.*, 2022, **24**, 13–35.
6 A. A. Taha, M. A. Shreadah, A. M. Ahmed and H. F. Heiba, *J. Environ. Chem. Eng.*, 2016, **4**, 1166–1180.
7 W. Bai, Z. Zhang, W. Tian, X. He, Y. Ma, Y. Zhao and Z. Chai, *J. Nanopart. Res.*, 2010, **12**, 1645–1654.
8 G. Da Costa Cunha, J. A. Peixoto, D. R. De Souza, L. P. C. Romão and Z. S. MacEdo, *Green Chem.*, 2016, **18**, 5342–5356.
9 A. Shahzad, W. Miran, K. Rasool, M. Nawaz, J. Jang, S. R. Lim and D. S. Lee, *RSC Adv.*, 2017, **7**, 9764–9771.
10 S. Panja, S. Hanson and C. Wang, *ACS Appl. Mater. Interfaces*, 2020, **12**, 25276–25285.
11 B. Alyüz and S. Veli, *J. Hazard. Mater.*, 2009, **167**, 482–488.
12 H. Cui, X. Huang, Z. Yu, P. Chen and X. Cao, *RSC Adv.*, 2020, **10**, 20231–20244.
13 W. Wang, R. Narain and H. Zeng, in *Polymer Science and Nanotechnology*, Elsevier, 2020, pp. 203–244.
14 T. Huang, H. G. Xu, K. X. Jiao, L. P. Zhu, H. R. Brown and H. L. Wang, *Adv. Mater.*, 2007, **19**, 1622–1626.
15 Y. Chen, W. Wang, D. Wu, M. Nagao, D. G. Hall, T. Thundat and R. Narain, *Biomacromolecules*, 2018, **19**, 596–605.
16 J. Chen, Q. Peng, T. Thundat and H. Zeng, *Chem. Mater.*, 2019, **31**, 4553–4563.
17 Y. Oladosu, M. Y. Rafii, F. Arolu, S. C. Chukwu, M. A. Salisu, I. K. Fagbohun, T. K. Muftaudeen, S. Swaray and B. S. Haliru, *Horticulturae*, 2022, **8**, 1–17.
18 F. Khan, M. Atif, M. Haseen, S. Kamal, M. S. Khan, S. Shahid and S. A. A. Nami, *J. Mater. Chem. B*, 2022, **10**, 170–203.
19 I. Altinbasak, S. Kocak, R. Sanyal and A. Sanyal, *Biomacromolecules*, 2022, **23**, 3525–3534.
20 T. Vermonden, R. Censi and W. E. Hennink, *Chem. Rev.*, 2012, **112**, 2853–2888.
21 N. Wu and Z. Li, *Chem. Eng. J.*, 2013, **215–216**, 894–902.
22 C. Zhao, G. Liu, Q. Tan, M. Gao, G. Chen, X. Huang, X. Xu, L. Li, J. Wang, Y. Zhang and D. Xu, *J. Adv. Res.*, 2023, **44**, 53–70.
23 A. H. Shalla, M. A. Bhat and Z. Yaseen, *J. Environ. Chem. Eng.*, 2018, **6**, 5938–5949.
24 S. Ahmad and S. Imran, *Mater. Adv.*, 2024, **5**, 8812–8825.
25 Z. Yuan, J. Wang, Y. Wang, Q. Liu, Y. Zhong, Y. Wang, L. Li, S. F. Lincoln and X. Guo, *RSC Adv.*, 2019, **9**, 21075–21085.
26 Y. Wang, X. Sun, Q. Liu and G. Yu, *Chem. Soc. Rev.*, 2025, **54**, 3475–3512.
27 K. C. Koehler, K. S. Anseth and C. N. Bowman, *Biomacromolecules*, 2013, **14**, 538–547.
28 H. Tamura, H. Nagahama and S. Tokura, *Cellulose*, 2006, **13**, 357–364.
29 E. G. Arafa, M. W. Sabaa, R. R. Mohamed, E. M. Kamel, A. M. Elzanaty, A. M. Mahmoud and O. F. Abdel-Gawad, *Carbohydr. Polym.*, 2022, **291**, 119555.
30 Z. Liu, Y. Wang, Y. Ren, G. Jin, C. Zhang, W. Chen and F. Yan, *Mater. Horiz.*, 2020, **7**, 919–927.
31 J. Yuan, D. Mecerreyes and M. Antonietti, *Prog. Polym. Sci.*, 2013, **38**, 1009–1036.
32 M. Zhu and Y. Yang, *Green Chem.*, 2024, **26**, 5022–5102.
33 R. Gracia, K. Vijayakrishna and D. Mecerreyes, *React. Funct. Polym.*, 2014, **79**, 54–58.
34 K. T. P. Charan, N. Pothanagandhi, K. Vijayakrishna, A. Sivaramakrishna, D. Mecerreyes and B. Sreedhar, *Eur. Polym. J.*, 2014, **60**, 114–122.
35 M. Isik, A. M. Fernandes, K. Vijayakrishna, M. Paulis and D. Mecerreyes, *Polym. Chem.*, 2016, **7**, 1668–1674.
36 N. Pothanagandhi, A. Sivaramakrishna and K. Vijayakrishna, *Polym. Chem.*, 2017, **8**, 918–925.
37 O. Lebedeva, D. Kultin and L. Kustov, *Green Chem.*, 2023, **25**, 9001–9019.
38 B. Tilottama and K. Vijayakrishna, *Macromolecules*, 2024, **57**, 3212–3222.
39 B. Tilottama, D. Nrusingha and K. Vijayakrishna, *J. Polym. Sci.*, 2025, **63**, 1086–1094.
40 B. Tilottama and K. Vijayakrishna, *Polym. Chem.*, 2024, **15**, 3529–3542.
41 J. Pinaud, K. Vijayakrishna, D. Taton and Y. Gnanou, *Macromolecules*, 2009, **42**, 4932–4936.
42 D. Ciolacu, A. M. Oprea, N. Anghel, G. Cazacu and M. Cazacu, *Mater. Sci. Eng., C*, 2012, **32**, 452–463.
43 P. Haripriya and K. Vijayakrishna, *Int. J. Biol. Macromol.*, 2024, **266**, 131230.
44 A. K. Saikia, S. Aggarwal and U. K. Mandal, *Int. J. Polym. Mater. Polym. Biomater.*, 2013, **62**, 39–44.
45 C. Yu, X. Chen, W. Zhu, L. Li, M. Peng, Y. Zhong, A. Naeem, Z. Zang and Y. Guan, *Gels*, 2022, **8**, 806.
46 X. Li, L. Cao and L. Chen, *Biochem. Eng. J.*, 2022, **187**, 108606.

47 C. Xiang, X. Zhang, J. Zhang, W. Chen, X. Li, X. Wei and P. Li, *J. Funct. Biomater.*, 2022, **13**, 140.
48 Z. Jiang, Q. Sun, Q. Li and X. Li, *Gels*, 2023, **9**, 1–15.
49 H. Li, C. wei Wu, S. Wang and W. Zhang, *Mater. Lett.*, 2020, **266**, 127504.
50 M. J. Moura, M. M. Figueiredo and M. H. Gil, *Biomacromolecules*, 2007, **8**, 3823–3829.
51 T. Xiang, T. Lu, W. F. Zhao and C. S. Zhao, *Langmuir*, 2019, **35**, 1146–1155.
52 S. Nöjd, P. Holmqvist, N. Boon, M. Obiols-Rabasa, P. S. Mohanty, R. Schweins and P. Schurtenberger, *Soft Matter*, 2018, **14**, 4150–4159.
53 R. Schroeder, A. A. Rudov, L. A. Lyon, W. Richtering, A. Pich and I. I. Potemkin, *Macromolecules*, 2015, **48**, 5914–5927.
54 B. A. Firestone and R. A. Siegel, *J. Appl. Polym. Sci.*, 1991, **43**, 901–914.
55 D. M. García, J. L. Escobar, N. Bada, J. Casquero, E. Hernáez and I. Katime, *Eur. Polym. J.*, 2004, **40**, 1637–1643.
56 J. Yang, K. Wang, Z. Lv, W. Li, K. Luo and Z. Cao, *ACS Omega*, 2021, **6**, 28285–28296.
57 H. Huang, L. Hou, F. Zhu, J. Li and M. Xu, *RSC Adv.*, 2018, **8**, 9334–9343.